Available online at www.sciencedirect.com
ScienceDirect
International Journal of Solids and Structures 44 (2007) 3601–3626
INTERNATIONAL JOURNAL OF SOLIDS and STRUCTURES
www.elsevier.com/locate/ijsolstr

Wave propagation and dynamic analysis of smoothly graded heterogeneous continua using graded finite elements

Zhengyu (Jenny) Zhang, Glaucio H. Paulino *

Department of Civil and Environmental Engineering, University of Illinois at Urbana-Champaign, Newmark Laboratory, 205 North Mathews Avenue, Urbana, IL 61801, USA

Received 21 January 2005
Available online 27 January 2007

Abstract

The dynamic behavior of smoothly graded heterogeneous materials is investigated using the finite element method. The global variation of material properties (e.g., Young's modulus, Poisson's ratio and mass density) is treated at the element level using a generalized isoparametric formulation. Three classes of examples are presented to illustrate this approach and to investigate the influence of material inhomogeneity on the characteristics of wave propagation pattern and stress redistribution. First, a cantilever beam example is presented for *verification* purposes. Emphasis is placed on the comparison of numerical results with analytical ones, as well as modal analysis for beams with different material gradation profiles. Second, wave propagation patterns are explored for a fixed-free slender bar considering homogeneous, bi-material, tri-layered and smoothly graded materials (steel/alumina), which also provide further verification of the numerical procedures. Comparison of stress histories in these samples indicates that the smooth transition of material gradation considerably alleviates the stress discontinuity in the bi-material system (with sharp interface). Third, a three-point-bending epoxy/glass graded beam specimen is investigated for *validation* purposes. The beam is graded along the height direction. Stress evolution history at a location of interest is analyzed in detail, which not only reveals the dependence of stress evolution on material gradation direction, but also provides information predictive of potential material failure time for graded beams with different material gradation profiles. Jointly, these three classes of examples provide proper verification and validation for the present numerical techniques.

Keywords: Finite element method; Graded finite element; Graded material; Heterogeneous materials; Dynamic analysis; Wave propagation; Generalized isoparametric formulation

1. Introduction

Materials possessing smoothly graded properties have drawn increasing attention in material science and industrial fields during the past decades due to their potential for providing improved performance in advanced engineering applications (Paulino et al., 2003). They maybe designed as functionally graded

* Corresponding author. Tel.: +1 217 333 3817; fax: +1 217 265 8041.
E-mail addresses: zzhang3@uiuc.edu (Z. Zhang), paulino@uiuc.edu (G.H. Paulino).

0020-7683/$ - see front matter © 2007 Elsevier Ltd. All rights reserved.
doi:10.1016/j.ijsolstr.2005.05.061

materials (FGMs) in which synthetic phases are graded to achieve desired properties and performance. For example, by smoothly interchanging the microstructural distribution of ceramic and metal phases in a graded material system, the resulting macro-structure takes advantage of desirable properties of both material constituents (e.g., hardness, corrosion resistance for ceramics and tensile strength, toughness for metals), and thus makes itself an excellent candidate for thermal protection applications (Chin, 1999; Suresh and Mortensen, 1998). Advanced material systems are frequently exposed to severe thermal/mechanical environments, and subjected to dynamic and impact loadings. In order to enhance material/structural performance under various dynamic loading conditions, it is essential to understand the system response and to identify critical instances (e.g., peak value of stress and failure initiation condition). Although a focus of academic and industrial interest, the dynamic behavior of this new generation of materials remains not well understood in relation to homogeneous or standard composites (e.g., laminates). Non-homogeneity of the material system introduces considerable complexity in the boundary value problem and demands intense investigation to reveal the role of material gradation on the system response. This work addresses some of the fundamental issues in the finite element modeling of graded material systems subjected to impact loading, and also investigates the influence of material non-homogeneity on the dynamic response.

The literature on the dynamic response of graded material systems subjected to dynamic loading is limited. The difficulty in obtaining analytical solutions for dynamic response of graded material systems is compounded by the *dispersive* nature of the heterogeneous material system, which is characteristic of elastodynamic response of material with continuously varying properties: "the pulse shape is distorted in time, the wave propagation speed is not constant, and there are no sharp interface that would cause wave reflections" (Chiu and Erdogan, 1999). Therefore, analytical or semi-analytical solutions are available only through a number of problems with simple boundary/initial conditions. Some problems with infinite/semi-infinite boundaries were solved using Laplace transforms. For instance, Whittier (1965) solved a slender bar with free–free ends and varying Young's modulus, Payton (1966) considered a semi-infinite rod subjected to a pressure step at its ends with several different wave speeds. Chiu and Erdogan (1999) solved a one-dimensional wave propagation in a functionally graded slab subjected to a pressure pulse with material gradation along the thickness direction. Their solution was obtained in wave summation form and they provided an example, which shows that there is considerable wave distortion in time. Banks-Sills et al. (2002) have performed dynamic finite element analyses of FGMs (Al 6061-TO and TiC) using ADINA (Bathe, 1999). Their investigation included simulation of discrete micro-structure, layer modeling and consideration of continuous change of material properties. Recently, Thamburaj et al. (2003) have implemented the damage model by Johnson and Holmquist (1994) into the dynamic finite element code DYNA3D (Gazonas, 2002), and investigated the effect of graded strength on damage propagation in continuously non-homogeneous materials. They observed that introducing different strength gradation can change the location of site of maximum damage, which may have important implication in the design of impact resistant materials and structures.

The numerical study on dynamic response of graded materials has been an active research area of recently. Reddy and his co-workers (Praveen and Reddy, 1998; Reddy, 2000; Reddy and Chin, 1998) studied plates of varying material properties through thickness using shear deformation plate theories employing von Karman non-linearity. Chakraborty and Gopalakrishnan (2003) developed the spectral finite element for wave analysis of functionally graded beams. Santare et al. (2003) compared the performance of both conventional and graded elements in an elastic wave propagation problem and pointed out that in general, the graded element outperforms the homogeneous element in capturing the smooth transition of stress field across element boundaries.

Few experimental data have been reported in literature for actual FGM specimens subjected to dynamic loading. Parameswaran and Shukla (1998, 2000) used photoelasticity technique to investigate dynamic fracture properties of a functionally graded material prepared by combining polyester resin and various amount of plasticizers. Rousseau and Tippur (2000, 2001a,b, 2002a,b) have conducted some dynamic experiments of polymer-based graded materials. These experimental data are employed in one of the simulations of this study, and our numerical results are compared with the experimental ones.

The remainder of this paper is organized as follows. First the temporal integration schemes used for dynamic analysis are described, followed by the graded element formulation for dynamic behavior of non-

homogeneous materials (Section 2). The numerical approach is both verified (i.e., the problem is solved correctly in mathematical sense using the described numerical scheme) and validated, i.e., to demonstrate that the analysis models the physical problem correctly by comparing the numerical solution with experimental observations (see, for example, Roache (1998)). Three classes of problems are investigated. First, a cantilever beam subjected to transverse transient point load is simulated to *verify* the numerical procedure by comparing the results to those from analytical solution and modal analysis (Section 3). Second, the wave propagation patterns in fixed-free bars with different material variation types: homogenous, bi-material, tri-layered and graded, are simulated to illustrate the relevance of material variation on the wave pattern (Section 4). This investigation provides further verification of the computational method. Third and finally, the stress evolution history for a three-point-bending beam subjected to impact loading is studied for *validation* purposes (Section 5). This investigation provides valuable insight on the prediction of structure bearing capacity (crack initiation) considering different material gradient cases. Finally, conclusions are inferred (Section 6).

2. Numerical scheme

In this section, the dynamic finite element formulation, the numerical aspects involving the dynamic updating scheme and treatment of material non-homogeneity are presented. The two-dimensional dynamic finite element formulation can be derived from the principle of virtual work, which is expressed as

$$\int_{\Omega}(\mathrm{div}\boldsymbol{\sigma}-\rho\ddot{\mathbf{u}})\delta\mathbf{u}\mathrm{d}\Omega-\int_{\Gamma}(\mathbf{T}-\boldsymbol{\sigma}\mathbf{n})\delta\mathbf{u}\mathrm{d}\Gamma=0 \tag{1}$$

where Ω represents domain area, Γ denotes boundary surface with normal vector $\mathbf{n}$, $\mathbf{u}$ is the displacement vector, $\mathbf{T}$ is the traction on the boundary, and $\boldsymbol{\sigma}$ is the Cauchy stress tensor. The superposed dots ($\ddot{\mathrm{u}}$) denote differentiation with respect to time, and ρ is the material density. By applying the divergence theorem and integration by parts to the general expression in (1), the following conventional expression can be obtained:

$$\int_{\Omega}(\boldsymbol{\sigma}:\delta\mathbf{E}+\rho\ddot{\mathbf{u}}\cdot\delta\mathbf{u})\mathrm{d}\Omega-\int_{\Gamma_{\mathrm{ext}}}\mathbf{T}_{\mathrm{ext}}\cdot\delta\mathbf{u}\mathrm{d}\Gamma=0 \tag{2}$$

where Γ_{ext} represents the boundary surface on which external traction $\mathbf{T}_{\mathrm{ext}}$ is applied, and $\mathbf{E}$ is the Green strain tensor.

2.1. Dynamic updating scheme

Both implicit and explicit updating schemes can be adopted to investigate the dynamic wave propagation problems. Usually implicit method is employed for long-term response analysis, while explicit method is preferred for transient dynamic analysis. In this study, explicit method is employed to capture the transient response of the dynamic system. In addition, modal analysis is carried out in Section 3. The widely used Newmark β method is described by (Newmark, 1959):

$$\mathbf{M}\ddot{\mathbf{u}}_{n+1}+\mathbf{K}\mathbf{u}_{n+1}=\mathbf{F}_{n+1} \tag{3}$$

$$\mathbf{u}_{n+1}=\mathbf{u}_n+\Delta t\dot{\mathbf{u}}_n+\frac{\Delta t^2}{2}(1-2\beta)\ddot{\mathbf{u}}_n+\beta\Delta t^2\ddot{\mathbf{u}}_{n+1} \tag{4}$$

$$\dot{\mathbf{u}}_{n+1}=\dot{\mathbf{u}}_n+(1-\gamma)\Delta t\ddot{\mathbf{u}}_n+\gamma\Delta t\ddot{\mathbf{u}}_{n+1} \tag{5}$$

where Δt denotes the time step, $\mathbf{M}$ is the mass matrix, $\mathbf{K}$ is the stiffness matrix, $\mathbf{F}$ is the external force vector, and parameters β and γ depend on the integration schemes employed. When $\beta=0$, $\gamma=1/2$, the method becomes the *explicit method*, or *central difference method*, which is conditionally stable with second order accuracy. The explicit updating scheme for nodal displacements, accelerations and velocities from time step (n) to ($n+1$) is given by the following expressions (see, for example, Hughes (1987))

$$\mathbf{u}_{n+1} = \mathbf{u}_n + \Delta t\dot{\mathbf{u}}_n + \frac{1}{2}\Delta t^2\ddot{\mathbf{u}}_n \tag{6}$$

$$\ddot{\mathbf{u}}_{n+1} = \mathbf{M}^{-1}(\mathbf{F}_{n+1} - \mathbf{R}_{\mathrm{int}_{n+1}}) \tag{7}$$

$$\dot{\mathbf{u}}_{n+1} = \dot{\mathbf{u}}_n + \frac{\Delta t}{2}(\ddot{\mathbf{u}}_n + \ddot{\mathbf{u}}_{n+1}) \tag{8}$$

where $\mathbf{R}_{\mathrm{int}}$ is the internal force vector obtained from $\mathbf{R}_{\mathrm{int}} = \mathbf{K}\mathbf{u}$.

2.2. Graded finite elements

To treat the material non-homogeneity inherent in the problem, we can use either homogeneous elements with constant material properties at the element level, which are evaluated at the centroid of each element (Fig. 1(a)), or graded elements, which incorporate the material property gradient at the size scale of the element (Fig. 1(b)). Kim and Paulino (2002) and Santare and Lambros (2000) developed the graded element concept with slightly different formulations. Both studies demonstrated that graded elements result in smoother and more accurate results than homogeneous elements for static problems. In this study, the scheme developed by Kim and Paulino (2002) is extended to dynamic problems. It employs the same shape functions to interpolate the unknown displacements, the geometry, and the material parameters, and hence assumes the name *Generalized Isoparametric Formulation (GIF)*. The interpolations for spatial coordinates (x, y), displacements (u, v) and material properties (E, v, ρ) are given by

$$x = \sum_{i=1}^{m} N_i\, x_i, \quad y = \sum_{i=1}^{m} N_i\, y_i \tag{9}$$

$$u = \sum_{i=1}^{m} N_i\, u_i, \quad v = \sum_{i=1}^{m} N_i\, v_i \tag{10}$$

$$E = \sum_{i=1}^{m} N_i\, E_i, \quad v = \sum_{i=1}^{m} N_i\, v_i, \quad \rho = \sum_{i=1}^{m} N_i\, \rho_i \tag{11}$$

respectively, where N_i are the shape functions, and m is the number of nodes per element. The variations of material property, e.g., Young's Modulus E, for homogeneous and graded elements are illustrated in Fig. 1.

By means of the principle of virtual work for the discretized finite element system, the element stiffness matrix and mass matrix are formulated as

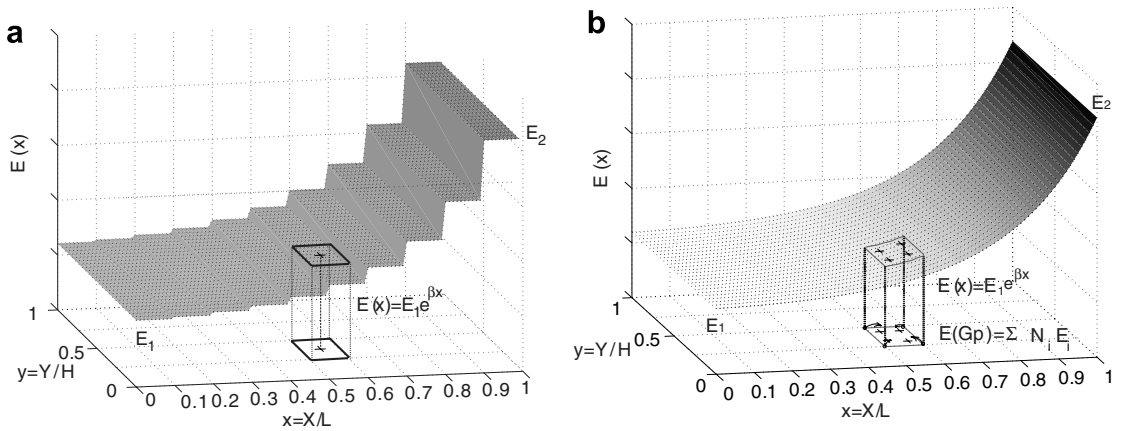

Fig. 1. Material property at the element level (exponential gradation along the Cartesian x direction for Young's modulus E is provided as example) – the symbols H and L denote height and length of a reference domain; (a) homogeneous element: material property evaluated at the element centroid is used for the entire element; (b) graded element: material property is first evaluated at element nodes and then interpolated to Gauss points (GP) using shape functions.

$$\mathbf{K}^{e} = \int_{\Omega^e} \mathbf{B}^T \mathbf{C}(\mathbf{x}) \mathbf{B} \mathrm{d}\Omega^e, \quad \mathbf{M}^{e} = \int_{\Omega^e} \mathbf{N}^T \boldsymbol{\rho}(\mathbf{x}) \mathbf{N} \mathrm{d}\Omega^e \tag{12}$$

where **B** denotes spatial derivatives of the shape function matrix **N**, and **C** is the constitutive material matrix. The above mass matrix is formulated as consistent mass matrix. As indicated in the classical book by Hughes (1987), the transient integration scheme and mass matrices are "matched" so that the induced period errors tend to cancel. For example, the match can be trapezoidal rule and consistent mass, or central differences and lumped mass. Therefore, in order to match the time integration scheme employed (central difference method), lumped mass matrix is formulated such that only diagonal elements are preserved and scaled to maintain the total mass:

$$\mathbf{M}^{e}_{\text{lump}} = \text{Diag}(\mathbf{M}^{e}_{\text{cons}}) \frac{\sum \mathbf{M}^{e}_{\text{cons}}}{\sum \text{Diag}(\mathbf{M}^{e}_{\text{cons}})} \tag{13}$$

where $\mathbf{M}^{e}_{\text{lump}}$ and $\mathbf{M}^{e}_{\text{cons}}$ stand for lumped and consistent mass matrices at the element level, respectively, and the operator Diag(·) extracts the diagonal elements of a matrix.

A dynamic finite element code is developed, and both homogeneous and graded elements are implemented, however, for the reasons given above, graded elements are preferred. It is evident from Fig. 1(a) and (b) that the graded elements approximate the material gradation much closer to the original material profile, with a smooth transition across element boundaries, while the material distribution across homogeneous element boundaries assumes a staircase-like profile. The use of graded elements is particularly beneficial within regions of coarse mesh and/or with high stress gradient.

2.3. Wave speed and time step control in graded materials

The stability of conventional explicit finite element schemes is usually governed by the Courant condition (Bathe, 1996), which provides an upper limit for the size of the time step Δt:

$$\Delta t \leqslant \ell_e / C_d \tag{14}$$

where ℓ_e is the shortest distance between two nodes in finite element mesh (Fig. 2), and the dilatational wave speed C_d is expressed in terms of the material elastic constants $E = E(\mathbf{x})$, $v = v(\mathbf{x})$, and density $\rho = \rho(\mathbf{x})$ as

$$C_d^2(\mathbf{x}) = \frac{E(\mathbf{x})(1 - v(\mathbf{x}))}{(1 + v(\mathbf{x}))(1 - 2v(\mathbf{x}))\rho(\mathbf{x})}: \quad \text{plane strain} \tag{15}$$

$$C_d^2(\mathbf{x}) = \frac{E(\mathbf{x})}{(1 - v^2(\mathbf{x}))\rho(\mathbf{x})}: \quad \text{plane stress.} \tag{16}$$

The above expressions of dilatational wave speed assume linear elasticity. Because the problems under study are restricted to linear elasticity, these expressions apply to the FEM formulation. However, since all material properties under consideration could vary in space, C_d is no longer a constant. To simplify the implementation, the varying wave speed is calculated depending on the profile of the material property, and a uniform limiting time step is used for the entire simulation.

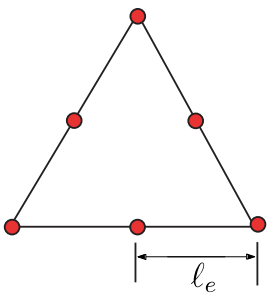

Fig. 2. Illustration of shortest distance between nodes for computing Δt (Courant condition).

3. Verification: cantilever beam

In this section, the modal analysis of a cantilever beam is carried out, and its response under transient point load is investigated for different material variation profiles. The results of this classical problem provide verification of the numerical approach. They also reveal some interesting characteristics particular to a graded cantilever beam.

First, the analytical solution for a homogeneous beam under transient point load is given. Next the Rayleigh–Ritz method is employed to evaluate the influence of material gradation profile on the natural frequencies and modes of the structure. This result is further verified with FEM modal analysis, which reveals some interesting features not captured by the standard one-dimensional (1D) Rayleigh–Ritz method. Finally, the responses of graded beams of different material gradation profile are compared, which are in agreement with predictions from the Rayleigh–Ritz method.

3.1. Problem description

Consider the cantilever beam illustrated by Fig. 3. The beam is of length $L = 2$ mm and height $H = 0.1$ mm (Fig. 3(a)). Transverse point load (Fig. 3(b)) is uniformly distributed along the free end of the beam, and consists of a sine pulse of duration T chosen as the period of the fundamental vibration mode of the cantilever beam, i.e.,

$$T = 2\pi/\omega_1 \tag{17}$$

where ω_1 is the fundamental frequency of the beam.

3.1.1. Homogeneous beam

The natural frequencies ω_i of the cantilever beam are given by (see, e.g., Chopra (1995))

$$\omega_i^2 = \lambda_i^4 \frac{EI}{\rho A}, \qquad \lambda_1 = 1.875/L, \quad \lambda_2 = 4.694/L, \quad \lambda_3 = 7.855/L, \cdots \tag{18}$$

where E, ρ, I and A denote the beam elastic modulus, density, moment of inertia and cross-sectional area, respectively. Moreover, λ_i is a general dimensional parameter that bears the relationship given by Eq. (18). The analytical solution for the tip deflection is given by Warburton (1976)

$$\begin{aligned} u(L,t) &= 4\frac{P}{M}\sum_{i=1}^{n}\left[\frac{1}{\omega_i}\int_0^l \sin\frac{\pi\tau}{T}\sin\omega_i(t-\tau)\mathrm{d}\tau\right] \quad \text{for } 0 \leqslant t \leqslant T \\ &= 4\frac{PL^3}{EI}\sum_{i=1}^{n}\left[\frac{\pi/(\omega_i T)}{(\lambda_i L)^4((\pi/\omega_i T)^2-1)}\left\{\begin{array}{l}(\cos\omega_i T+1)\sin\omega_i(t-T)\\ +\sin\omega_i T\cos\omega_i(t-T)\end{array}\right\}\right] \text{for } t \geqslant T \end{aligned} \tag{19}$$

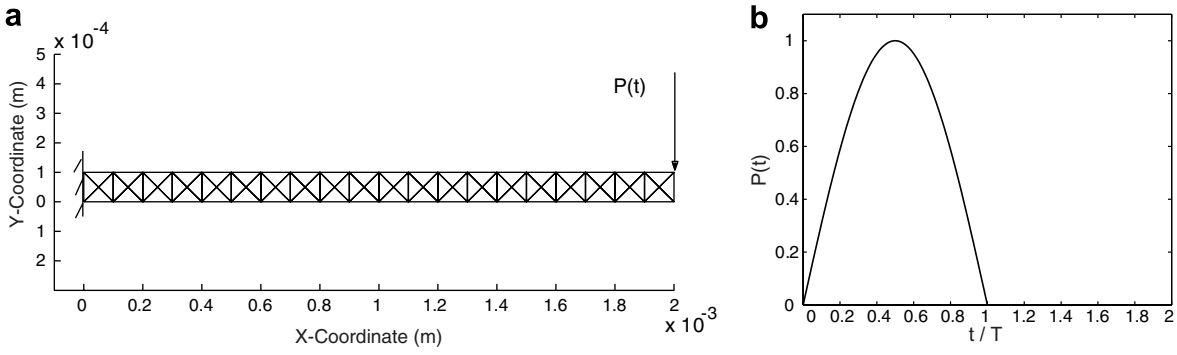

Fig. 3. (a) Geometry and FEM discretization (203 nodes, 80 T6 elements) of cantilever beam; (b) normalized load history.

where $M = \rho A$ denotes the total mass of the beam. The T6 elements, with mesh discretization shown in Fig. 3(a), produce very good results compared with the analytical solution expressed by Eq. (19), as demonstrated in Fig. 4, which shows that both results agree with plotting accuracy.

3.1.2. Graded beams

The material gradation for the graded cantilever beam (see Fig. 3) is considered along either x or y direction (Fig. 5). For each direction, three material gradation profiles are considered: exponential, linear and equivalent homogeneous, which can be expressed as follows (assume material properties vary in x direction).

For exponential material gradation

$$E(x) = E_1 e^{\alpha x}, \quad \rho(x) = \rho_1 e^{\beta x}, \quad v(x) = v_1 e^{\gamma x} \tag{20}$$

where α, β and γ are the material gradation parameters for E, ρ and v, respectively.

For linear material variation

$$\begin{aligned} E(x) &= E_1 + (E_2 - E_1)x/L \\ \rho(x) &= \rho_1 + (\rho_2 - \rho_1)x/L \\ v(x) &= v_1 + (v_2 - v_1)x/L \end{aligned} \tag{21}$$

where the subscripts 1 and 2 denote the two endpoints $x = 0$ and $x = L$, respectively.

For equivalent homogeneous beam

$$\overline{E} = \frac{1}{A}\int E(x)\mathrm{d}A, \quad \overline{\rho} = \frac{1}{A}\int \rho(x)\mathrm{d}A, \quad \overline{v} = \frac{1}{A}\int v(x)\mathrm{d}A \tag{22}$$

which are defined as the equivalent material constants.

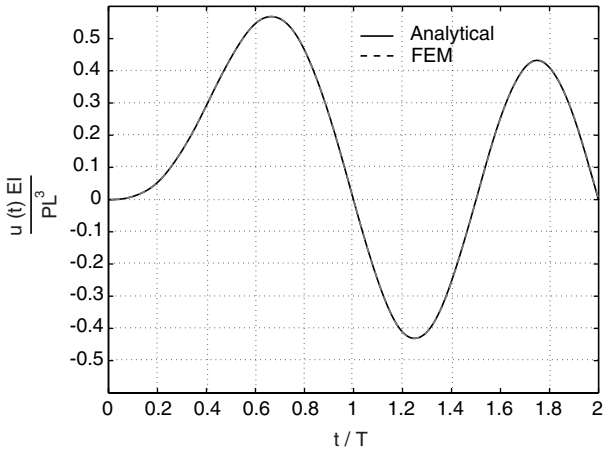

Fig. 4. Normalized displacement of homogeneous cantilever beam.

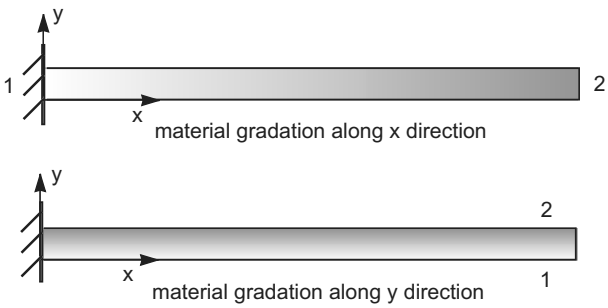

Fig. 5. Beams with material gradation along the x and y directions, respectively.

3.2. Modal analysis

As the dynamic response of any system can be decomposed by combining its basic modes, the modal analysis provides fundamental dynamic characteristics of the system. Two approaches are adopted to perform the modal analysis, the Rayleigh–Ritz method and the finite element method, and the results are compared.

3.2.1. Rayleigh–Ritz method

By simplifying the cantilever beam as a 1D problem with material variation along x direction, one obtains the governing equation

$$\frac{\partial^2}{\partial x^2}[E(x)I\frac{\partial^2}{\partial x^2}q(x,t)] + \rho(x)A\frac{\partial^2}{\partial t^2}q(x,t) = f(x,t) \tag{23}$$

where $q(x,t)$ is the beam response under load $f(x,t)$. To solve the eigenvalue problem, we set $f(x,t) = 0$, and consider $q(x,t)$ harmonic in time, i.e.,

$$q(x,t) = u(x)\mathrm{e}^{\mathrm{i}\omega t} \tag{24}$$

where ω is frequency and $u(x)$ is the corresponding mode shape. By introducing the energy conservation concept (Meirovitch, 1967), we obtain the Rayleigh's quotient

$$R(u) = \omega^2 = \frac{\int_0^L E(x)I[u''(x)]^2\mathrm{d}x}{\int_0^L \rho(x)A(u(x))^2\mathrm{d}x} = \frac{N(u)}{D(u)}. \tag{25}$$

If the function u chosen for expression (25) happens to be a true mode function, the frequency (ω) solved for will be the corresponding actual frequency. The stationarity of the Rayleigh quotient states that *"the frequency of vibration of a conservative system vibrating about an equilibrium position has a stationary value in the neighborhood of a natural mode"* (Meirovitch, 1967), hence we can construct trial mode functions and minimize the Rayleigh's quotient. A trial mode function can be constructed as

$$u_n(x) = \sum_{i=1}^{n} a_i\phi_i(x)$$

where a_i are coefficients to be determined and ϕ_i are admissible functions that satisfy all the essential boundary conditions

$$\phi(0) = 0, \quad \phi'(0) = 0. \tag{26}$$

The necessary conditions for the minimum of the Rayleigh's quotient are

$$\frac{\partial R(u)}{\partial a_j} = 0, \text{ or } \frac{\partial N(u)}{\partial a_j} - \lambda\frac{\partial D(u)}{\partial a_j} = 0, \quad j = 1,2,\cdots,n \tag{27}$$

where λ is defined as the minimum estimated value of the Rayleigh's quotient (Eq. (27)), i.e.,

$$\min(R(u)) = \lambda.$$

By introducing symmetric stiffness and mass matrices $\mathbf{K}$ and $\mathbf{M}$:

$$\mathbf{K}_{ij} = \int_0^l E(x)I\frac{\partial\phi_i(x)}{\partial x}\frac{\partial\phi_j(x)}{\partial x}\mathrm{d}x, \quad \mathbf{M}_{ij} = \int_0^l \rho(x)A\phi_i(x)\phi_j(x)\mathrm{d}x, \tag{28}$$

$N(u)$ and $D(u)$ can be written in terms of these matrices as follows

$$N(u) = \sum_{i=1}^{n}\sum_{j=1}^{n}\mathbf{K}_{ij}a_ia_j, \quad D(u) = \sum_{i=1}^{n}\sum_{j=1}^{n}\mathbf{M}_{ij}a_ia_j. \tag{29}$$

Introducing (29) into (27) and recalling the symmetry of the coefficients $\mathbf{K}_{ij}$, $\mathbf{M}_{ij}$, we obtain

$$\sum_{j=1}^{n}(\mathbf{K}_{rj} - \lambda \mathbf{M}_{rj})a_j = 0, \quad r = 1, 2, \cdots, n. \tag{30}$$

which represents a set of n homogeneous algebraic equations in the unknowns a_j. Note that $\lambda = \omega^2$ render the linear Eq. (30) into matrix form

$$\mathbf{K} = \omega^2 \mathbf{M} \tag{31}$$

We can solve for the natural frequencies and corresponding modes, and the frequencies ω provide upper bounds for the true frequencies ω^* (Meirovitch, 1967):

$$\omega_r \geqslant \omega_r^* \quad r = 1, 2, \cdots, n \tag{32}$$

The base functions chosen for the graded cantilever beams under consideration are the polynomial series:

$$\phi_1(x) = x^2, \quad \phi_2(x) = x^3, \quad \phi_3(x) = x^4, \quad \phi_4(x) = x^5 \cdots \tag{33}$$

By incorporating more terms in the formulation, the Rayleigh–Ritz method guarantees that, with a complete set of base functions, the solution approaches the exact result asymptotically. The results listed in Tables 1–3 are obtained for material properties

$$E_l = 1 \text{ GPa}, E_h = 5 \text{ GPa}; \quad \rho_l = 0.5 \text{ g/cm}^3, \ \rho_h = 1.5 \text{ g/cm}^3 \tag{34}$$

where subscript l denotes the side where material elastic constants are lower, and h where it is higher.

In Tables 1–3, *SoftLHS*, *StiffLHS* and *Equiv.* denote the cases where the beam is softer (E_l, ρ_l) at the clamped end, stiffer (E_h, ρ_h) at the clamped end, and equivalent homogeneous beam as defined in Eq. (22). It is apparent that the beam which is softer at the clamped end has smaller natural frequency, and thus the whole structure is more compliant than the case where the beam is stiffer at the clamped end. According to Fig. 6, the equivalent homogeneous result is in between the other two, however, it is not simply the average of the two. Moreover, the influence of the material gradation function (exponential and linear) is not as significant (cf. results from either Table 1, 2 or 3).

Table 1
Natural frequency ω_1 for graded beam and equivalent homogeneous beam considering gradation along x direction (obtained from Rayleigh–Ritz method)

Num. of base functions	ω_1 ($\times 10^4$)					
	Exponential variation			Linear variation		
	SoftLHS	StiffLHS	Equiv.	SoftLHS	StiffLHS	Equiv.
2	2.7934	6.0983	4.2128	3.0405	6.2166	4.4159
3	2.6516	6.0705	4.1942	2.8388	6.2153	4.3963
4	2.6477	6.0673	4.1929	2.8183	6.2138	4.3950
5	2.2425	6.0666	4.1929	2.3823	6.2137	4.3950
6	2.2423	6.0655	4.1929	2.3816	6.2137	4.3950
Analytical	–	–	4.1929	–	–	4.3950

Table 2
Natural frequency ω_2 for graded beam and equivalent homogeneous beam considering gradation along x direction (obtained from Rayleigh–Ritz method)

Num. of base functions	ω_2 ($\times 10^4$)					
	Exponential variation			Linear variation		
	SoftLHS	StiffLHS	Equiv.	SoftLHS	StiffLHS	Equiv.
2	46.479	36.856	41.508	47.063	38.972	43.509
3	23.842	29.600	26.514	25.332	30.936	27.792
4	22.428	29.140	26.424	23.837	30.785	27.697
5	22.425	29.000	26.277	23.823	30.685	27.544
6	22.423	28.971	26.277	23.816	30.675	27.543
Analytical	–	–	26.277	–	–	27.543

Table 3
Natural frequency ω_3 for graded beam and equivalent homogeneous beam considering gradation along x direction (obtained from Rayleigh–Ritz method)

Num. of base functions	ω_3 ($\times 10^4$)					
	Exponential variation			Linear variation		
	SoftLHS	StiffLHS	Equiv.	SoftLHS	StiffLHS	Equiv.
3	168.62	114.65	140.89	167.70	118.71	147.68
4	73.990	79.009	75.542	77.142	82.066	79.183
5	69.346	76.547	75.414	72.671	80.779	79.050
6	68.793	75.224	73.598	72.428	79.645	77.145
7	68.680	74.948	73.596	72.415	79.521	77.144
8	68.676	74.945	73.575	72.407	79.519	77.122
Analytical	–	–	73.580	–	–	77.126

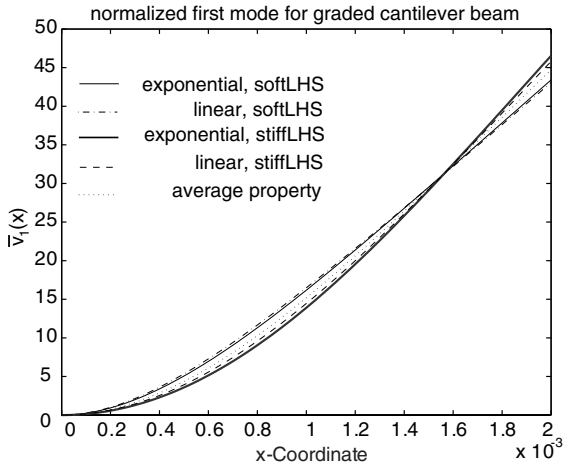

Fig. 6. Normalized 1st mode shapes of cantilever beams (Rayleigh–Ritz method).

The analytical solution for the equivalent homogeneous beams in Tables 1–3 are obtained by substituting averaged material properties (22) into Eq. (18). Clearly the Rayleigh–Ritz method gives excellent estimation of lower frequencies with only a few base functions for this case, and for FGM beams the frequencies also converge reasonably fast. However, for the higher modes we expect that more base function terms are needed. Since the Rayleigh–Ritz method is usually employed to obtain lower frequencies, the present study is limited up to the 3rd mode.

The first two mode shapes of the structure are plotted in Figs. 6 and 7. The normalized mode shape is defined as

$$\overline{v}_i(x) = \frac{v_i(x)}{\sqrt{\int_0^L v_i^2(x)\mathrm{d}x}} \tag{35}$$

where $v_i(x)$ is the ith mode shape before normalization. The first mode is similar for all material gradation cases (Fig. 6), while for the higher mode the difference is more noticeable (Fig. 7). The Rayleigh–Ritz method provides better estimation of frequencies than mode shapes. We will reexamine the results by comparison with FEM results in the next section.

3.2.2. Comparison of modes from Rayleigh–Ritz and FEM

As an alternative approach to obtain the natural frequencies and modes, modal analysis is performed using FEM. The global stiffness matrix **K** and mass matrix **M** are assembled, and boundary conditions are introduced. Then the following system is solved

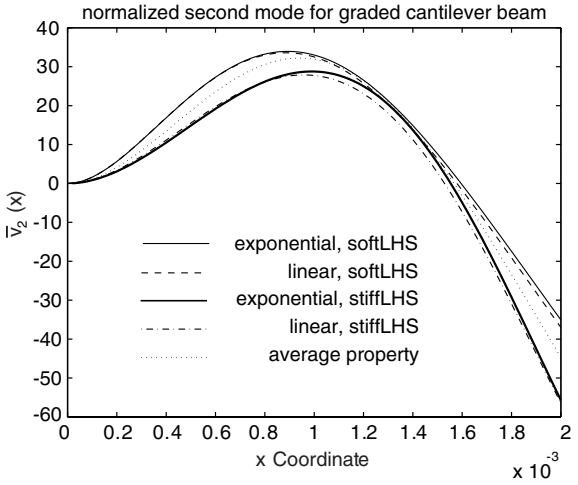

Fig. 7. Normalized 2nd mode shapes of cantilever beams (Rayleigh–Ritz method).

$$\mathbf{Ku} - \omega^2 \mathbf{Mu} = \mathbf{0}. \tag{36}$$

Six natural frequencies are provided in Table 4 for graded beams and equivalent homogeneous beams, each with different material gradation profiles. The corresponding mode shapes are plotted in Figs. 8–10. Some conclusions can be drawn from the results:

- Comparison of Table 4 and Tables 1–3 reveals that the results from the two methods (Rayleigh–Ritz and FEM) are in reasonably good agreement. Some of the differences are a consequence of modeling the 2D structure using a 1D model with the Rayleigh–Ritz method employed in the previous section. When a 2D structure is simplified as a 1D model, the Poisson ratio effect is ignored.
- The trend of influence of material gradation on frequency is consistent with the conclusion from the Rayleigh–Ritz method, i.e., the beams softer at the clamped end are more compliant than the beams stiffer at the clamped end, thus producing smaller frequencies compared to the latter. For material gradation along y direction, the results are close to those of the equivalent homogeneous beams.
- The influence of material variation magnitude on frequency is more significant for the lower modes than for higher modes. For example, for an exponentially graded beam under mode 1, the frequency for *SoftLHS* is 2.3 times of that for *StiffLHS* (6.055/2.649 = 2.29), while at mode 6, the ratio is merely 1.029 (217.14/211.04).

A longitudinal vibration mode is found in the 2D FEM analysis. This mode occurs as 4th mode for both the beam softer at the clamped end (Fig. 8(d)) and the equivalent homogeneous beam (not reported in the paper), while it occurs as 5th mode for the beam stiffer at the clamped end (Fig. 9(e)). This indicates that different material gradation profiles can change the sequence of some particular modes. A similar mode shape occurs for beams graded along y direction as 5th mode (Fig. 10), yet it is not purely elongation–compression along x

Table 4
First six natural frequencies ($\omega_i, i = 1, \ldots, 6$) for graded beams and equivalent homogeneous beam from FEM modal analysis

ω ($\times 10^4$)	Exponential variation				Linear variation			
	SoftLHS	StiffLHS	Y_grad	Equiv.	SoftLHS	StiffLHS	Y_grad	Equiv.
ω_1	2.649	6.055	3.882	4.190	2.816	6.204	4.055	4.392
ω_2	22.15	28.63	24.08	25.97	23.52	30.31	25.16	27.22
ω_3	66.70	72.83	66.38	71.51	70.31	77.25	69.39	74.96
ω_4	93.86	136.36	127.19	129.89	100.20	144.48	133.13	136.15
ω_5	130.27	162.41	130.00	136.94	137.29	169.56	136.21	143.54
ω_6	211.04	217.14	205.04	220.16	222.47	229.82	214.70	230.77

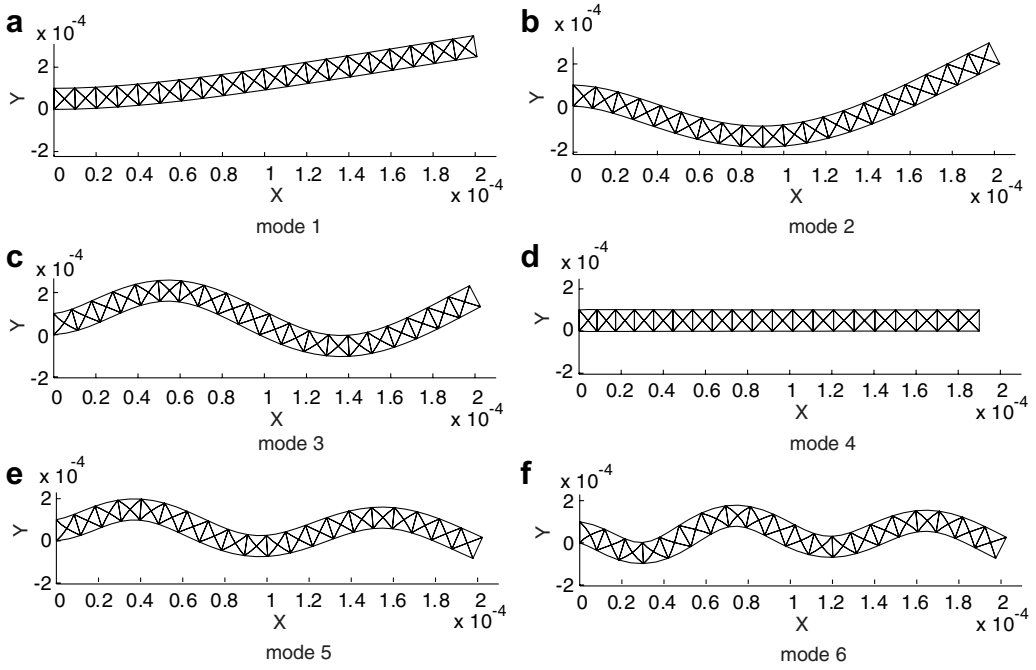

Fig. 8. Six mode shapes of graded cantilever beam, linear gradation along x direction, softer at clamped end (SoftLHS), $E_2/E_1 = 5$, $\rho_2/\rho_1 = 3$.

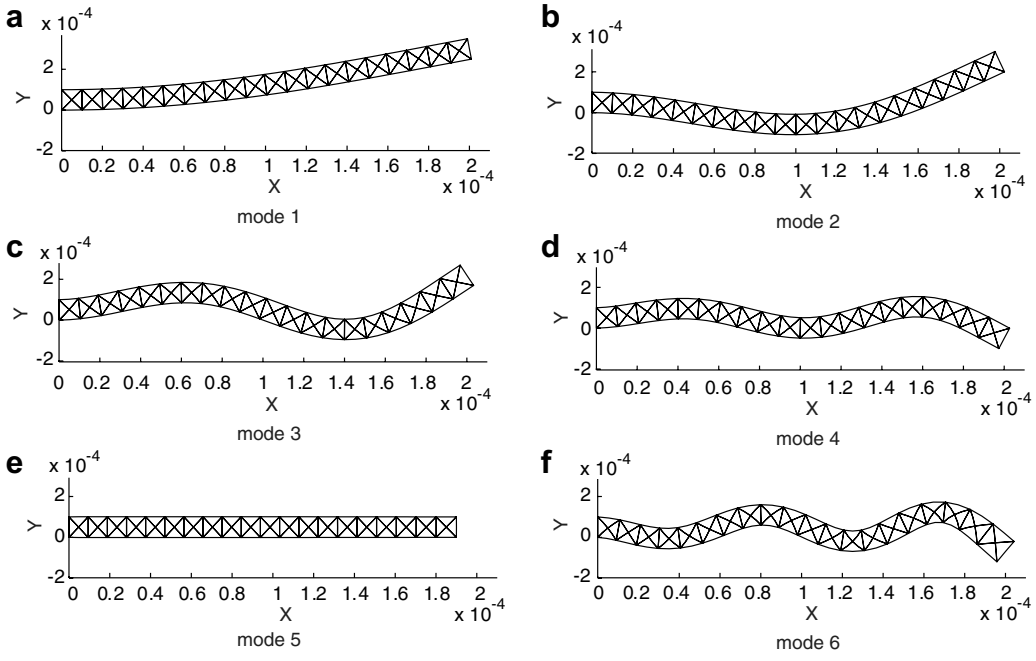

Fig. 9. Six mode shapes of graded cantilever beam, linear gradation along x direction, stiffer at clamped end (StiffLHS), $E_2/E_1 = 1/5$, $\rho_2/\rho_1 = 1/3$.

direction, but rather accompanied with bending in y direction (as expected). This behavior is induced by the non-symmetric material distribution along the height direction of the beam, which prevents the beam from displaying a deformation pattern purely along the x direction.

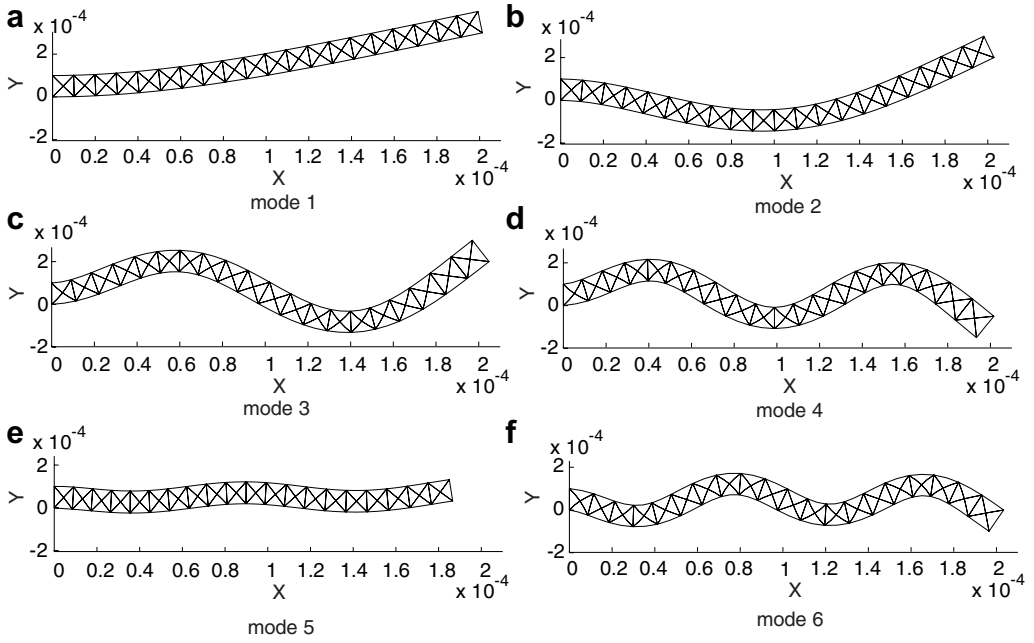

Fig. 10. Six mode shapes of graded cantilever beam, linear gradation along y direction, $E_2/E_1 = 5$, $\rho_2/\rho_1 = 3$.

The Rayleigh–Ritz method performed in the previous section is unable to catch the longitudinal mode shape, since the polynomial base functions can only give rise to deformation in y direction. This is inherent to the base functions we choose, however, and the Rayleigh–Ritz method still proves to be remarkably efficient and accurate for obtaining the lower frequencies and mode shapes for graded beams.

3.3. Graded cantilever beams subjected to transient point load

Under the tip point load (Fig. 3(b)), where the period T is the fundamental period of each graded beam, the response of the cantilever beam is dominated by the first mode behavior. This can be clearly observed from Fig. 11, where all beam responses match the 1st natural frequency. At $t > T$, when transient force vanishes, the free vibration of each beam follows its own fundamental period, and its amplitude is scaled with respect

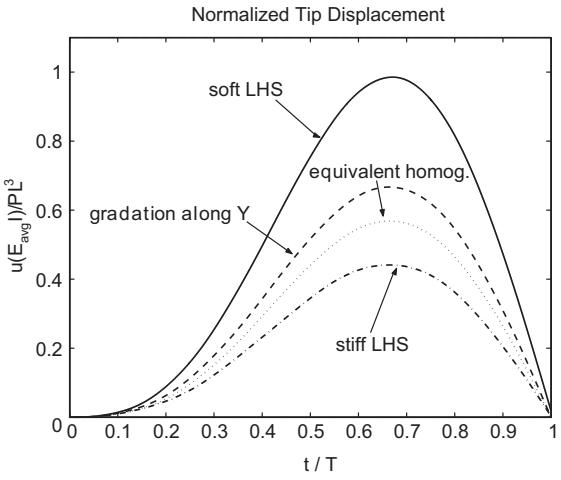

Fig. 11. Normalized tip displacement of graded cantilever beams under transient sine curve load (Fig. 3(b)). For the graded beams, the material changes linearly with modulus contrast of 5 and density contrast of 3.

to the amplitude at $t < T$ in the same manner as the analytical solution in Fig. 4. The deflection amplitude of beams with different material gradations are in agreement with the observation in the previous section, i.e., beam softer at the clamped end has larger deflection; beam stiffer at the clamped end has smaller deflection; beam graded along y direction and equivalent homogeneous beam are in between the other two, while beam graded along y direction is more compliant than equivalent beam.

4. Verification: one-dimensional wave propagation

Transient wave propagation along a fixed-free bar is investigated considering homogeneous, bi-material, and graded material properties along the height direction. The objective of this example is to investigate the influence of material gradation on the wave propagation pattern.

4.1. Problem description

Consider the fixed-free slender bar illustrated in Fig. 12(a). The bar is of length $L = 1$ m, and height $H = 0.05$ m. A transient axial loading with high frequency (Fig. 12(b)) is applied across the right free surface of the bar, which consists of a sine pulse of duration 50 μs. The fundamental period is $T = 0.0174$ s.

Four material gradation cases along the beam height are considered: homogeneous, bi-material, tri-layered and smoothly graded, as shown in Fig. 13(a)–(d), respectively. The material system under consideration is taken as: steel for homogeneous bar, steel/alumina for both bi-material and graded bars. The material properties for steel and alumina are provided in Table 5. For bi-material bar, the cross section is made of steel in the upper half and alumina in the lower half, with a sharp interface in the middle. For the tri-layered bar, the cross section is made of steel in the upper layer, alumina in the lower layer, and smooth transition layer in between. For graded regions, material property varies linearly from pure steel at upper surface to pure alumina at lower surface.

4.2. Mesh size control

High order modes participate in the bar response of Fig. 12, which in turn requires refined element size (Chakraborty and Gopalakrishnan, 2003). To capture the transient response, the time step needs to be small

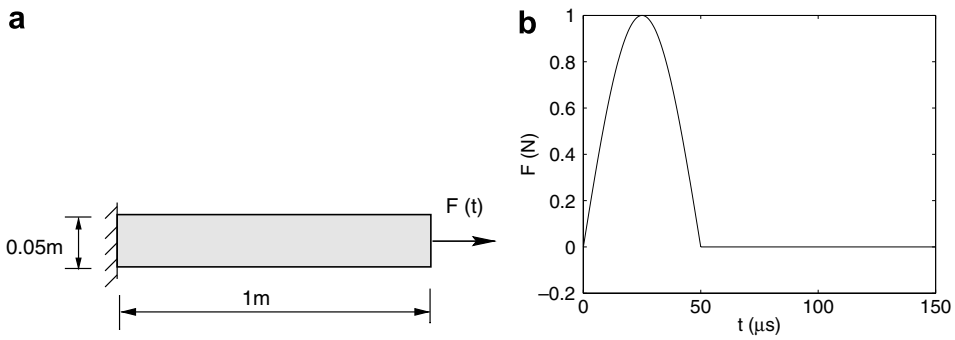

Fig. 12. Geometry and applied force for a fixed-free thin bar; (a) geometry; (b) applied load history.

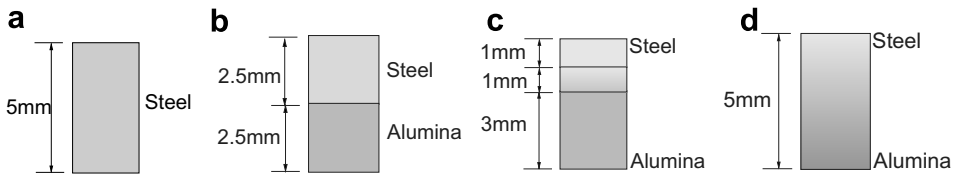

Fig. 13. Bar cross section material property; (a) homogeneous bar; (b) bi-material bar; (c) tri-layered bar; (d) graded bar.

Table 5
Steel and alumina material properties

Material	E (GPa)	ν	ρ (kg/m^3)	C_d (m/s)
Steel	210	0.31	7800	6109
Alumina	390	0.22	3950	10617

enough in order to track the change of applied load, and adequate element size can be estimated according to the Courant condition. For example, when the applied force period is discretized into 100 time steps, the corresponding element size is

$$h = C_d \times \Delta t = 6109 \times \frac{50 \times 10^{-6}}{100} = 3.06 \times 10^{-3}\text{m} = 3.06\ \text{mm}. \tag{37}$$

Taking into account material gradation along the height direction, the bar of Fig. 12(a) is discretized into 300×15 quads, each divided into 4 T6 elements. This leads to a mesh with 36,631 nodes and 18,000 T6 elements, which is used for the wave propagation problem.

4.3. Results and discussions

The analytical solution for a 1D stress wave propagation is given by Meirovitch (1967)

$$\sigma(x,t) = \sigma^0 f\left(t + \frac{x}{C_d}\right) + \hat{\sigma}^0 f\left(t - \frac{x}{C_d}\right) \tag{38}$$

where the first and second term on the right hand side indicate the left-traveling-wave and the right-traveling-wave, respectively. The parameters σ^0 and $\hat{\sigma}^0$ are the magnitude of the impact stress $f(t)$, while the sign depends on the boundary condition where the wave impacts. When the stress wave reaches a fixed end, the stress magnitude doubles while the velocity changes sign; when the stress wave reaches a free end, the stress vanishes while the velocity doubles.

The numerical simulations employ 2D finite elements. Thus the current numerical model is not 1D in nature, however it reasonably resembles a 1D case as the bar is slender. Therefore, we set the analytical solution of the homogeneous bar as a reference result to which the numerical results are compared. Because the bars under consideration possess different material properties, the results reported are normalized in order to provide meaningful comparison. Therefore, stress is reported as σ/σ^0 and time as $t \times C_d/L$.

4.3.1. Homogeneous bar

In 1D homogeneous case, the stress wave propagates at constant speed and retains its initial shape. This is shown in Fig. 14. Three locations along the beam are chosen to represent the stress wave behavior. The free end ($x = L$) experiences the stress wave which retains its shape, and afterwards this boundary becomes stress-free, as shown in Fig. 14 with the solid ($x = L$) curve. The stress wave travels across point $x = 0.5L$ (dash curve) at normalized time $t' = t \times C_d/L = 0.5$, and impacts the fixed end point $x = 0$ (dash-dot curve) at $t' = 1$, at which its magnitude is doubled. The wave reflects back, passes $x = 0.5L$ position, and reaches the free end at $t' = 2$. In the next cycle (normalized time $t' = 2$–4), the wave becomes compressive wave, and travels towards the fixed end and reflects back following similar pattern as described between normalized time $t' = 0$–2. The numerical result is also compared with the 1D analytical solution in Fig. 14. It is clearly shown that the shape and magnitude of numerical results follow closely with the analytical solution. However, there are small fluctuations in the 2D simulation which are absent from the 1D analytical solution. When Poisson ratio $\nu = 0$, the problem becomes 1D and the upper and lower boundaries do not move. In the 2D simulation, as stress front propagates, the Poisson ratio effect results in constant vertical fluctuation of the upper and lower boundaries, which in turn induces fluctuation in stress wave. The difference in period is due to the negligence of the Poisson ratio effect in the 1D analytical solution. To verify the above statement, another simulation using Poisson ratio $\nu = 0$ is carried out. The amplitude and period of the numerical result matches the analytical solution, as shown in Fig. 15.

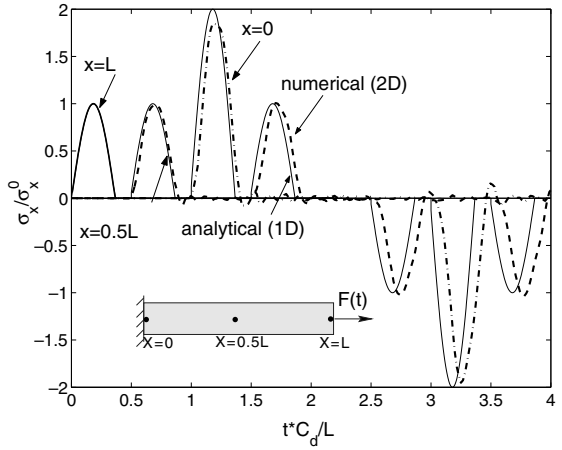

Fig. 14. Stress history for homogeneous bar (2D simulation) subjected to transient loading and its comparison with 1D analytical solution; numerical results obtained at points $x = L$ (thick solid line), $x = 0.5L$ (dashed line) and $x = 0$ (dash-dot line); 1D analytical results (thin solid line) obtained for the same three points.

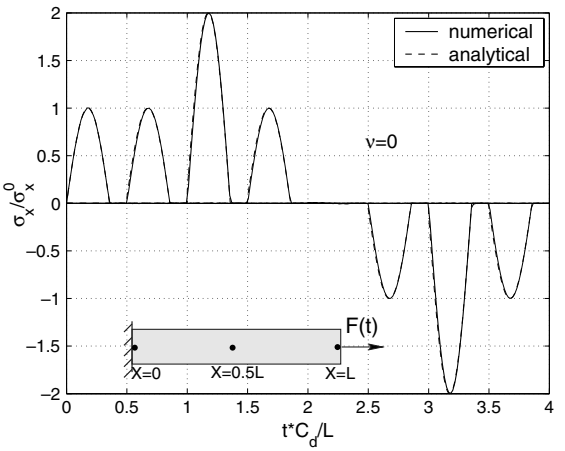

Fig. 15. Comparison of 2D numerical results (solid line) with 1D analytical results (dashed line) for the same three points in Fig. 14 when Poisson ratio $v = 0$.

4.3.2. Bi-material bar

For bi-material system, stress jump is present at the interface between two material phases. The results plotted in Fig. 16 compare the stress history of three pairs of nodes residing across the material interface, at locations x=0, $0.5L$ and L, respectively. Apparently, stress travels at the same speed along x direction inside the two phases, as it reaches peaks at the same time intervals for each pair of nodes. The magnitude differ, as expected, since the stiffer side sustains higher stress. Compared to the homogeneous case, the stress magnitude is lower at the steel side, and higher at the alumina side. Fluctuations are more noticeable than the homogeneous case due to the reflected wave at the material interface that compounds the wave pattern. Although the wave speed is different for the two material phases, the faster one "*drags*" the slower one and the wave propagates at the wave speed of alumina.

4.3.3. Tri-layer bar with thin graded interface

For the tri-layer bar, the graded middle layer ($y = 3$–4 mm) provides smooth transition for material variation from top layer (steel, $y = 4$–5 mm) to bottom layer (alumina, $y = 0$–3 mm). Since there are no distinctive interfaces between these layers, stress jump is alleviated compared to the bi-material case. The results plotted in Fig. 17 compare the stress history of three groups of nodes residing at the upper ($y = 4$ mm), middle

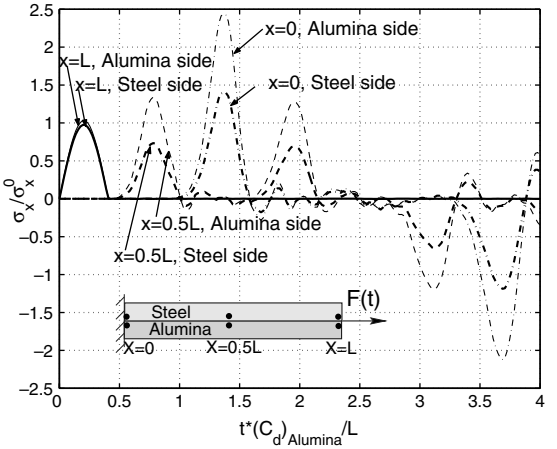

Fig. 16. Stress history of 6 points (indicated by solid dots in the insert) on a bi-material bar subjected to transient loading. Solid, dashed and dash-dot lines indicate points at $x = L$, $0.5L$ and 0, respectively. Thin and thick lines indicate points at alumina and steel side, respectively.

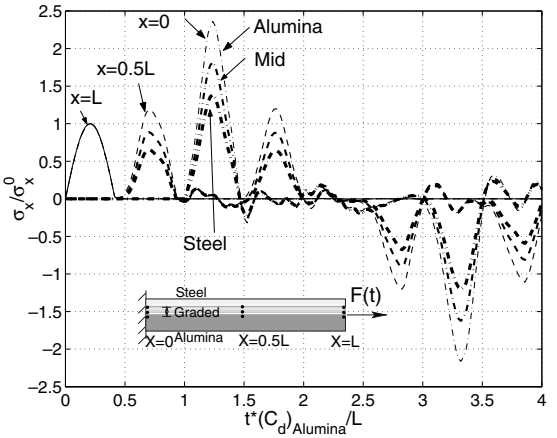

Fig. 17. Stress history of 9 points (indicated by solid dots in the insert) on a tri-layer bar subjected to transient loading. Solid, dashed and dash-dot lines indicate points at $x = L$, $0.5L$ and 0, respectively. Thin, intermediate-thick and thick lines indicate alumina-rich side, mid-plane and steel-rich side of the graded interface, respectively.

($y = 3.5$ mm) and lower ($y = 3$ mm) positions of the graded layer, at locations x=0, $0.5L$ and L, respectively. Apparently, stress travels at the same speed along x direction, and the stiffer side sustains higher stress.

4.3.4. Graded bar

Due to the gradual variation of material gradation, stress jump does not occur, but varies smoothly along the height direction. The results plotted in Fig. 18 compare the stress history of three groups of nodes residing at the upper, lower and middle surface, at locations x=0, $0.5L$ and L, respectively. Similarly to the bi-material case, the wave that moves fastest "*drags*" the rest to move along, so at the monitored points of same x location, the peak values occur simultaneously. At the free end, despite the material difference, the stress surges across the entire bar height with the same magnitude (since this is the initial boundary condition prescribed). The stress magnitude differ noticeably at other places, especially at the fixed end, where the alumina-rich side experience much higher stress than the opposite side. Also, the fluctuation is even more significant, due to the large number of wave tides that travel at different speeds.

4.3.5. Stress contour

Stress contours provide more instinctive image of the wave pattern. The stress distribution inside the bar at certain time instant is shown for the three bars discussed above in Fig. 19. It clearly reveals a stress jump along

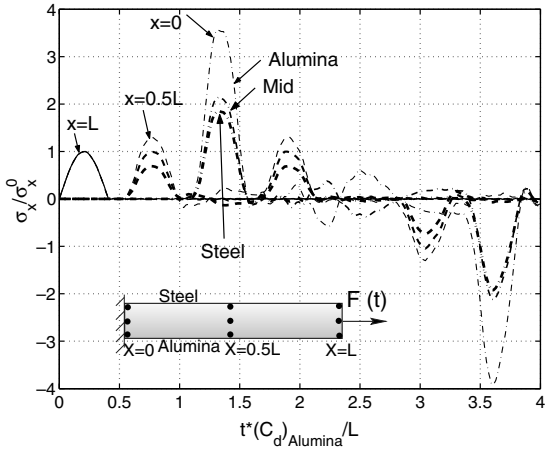

Fig. 18. Stress history of 9 points (indicated by solid dots in the insert) on a graded beam subjected to transient loading. Solid, dashed and dash-dot lines indicate points at $x = L$, $0.5L$ and 0, respectively. Thin, intermediate-thick and thick lines indicate alumina-rich side, mid-plane and steel-rich side, respectively.

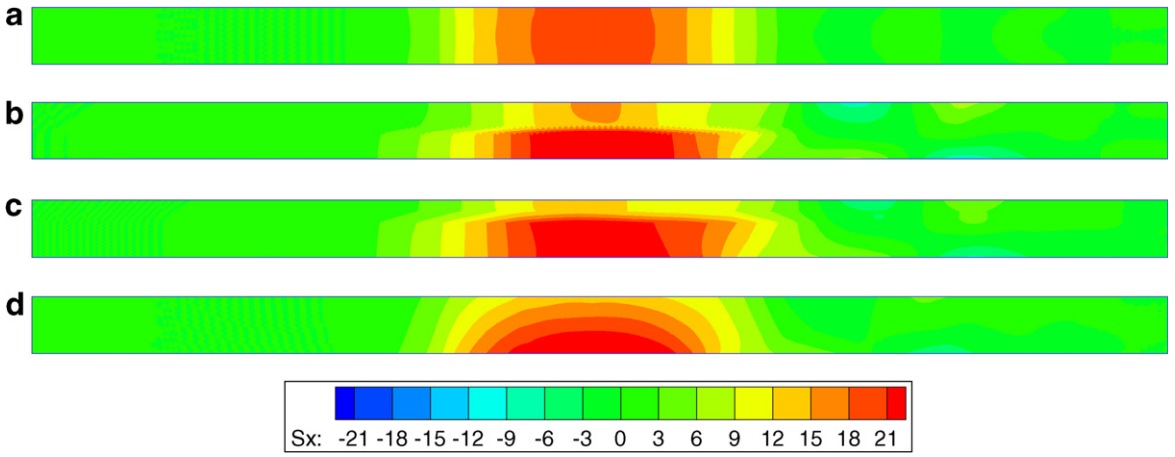

Fig. 19. Comparison of stress contours (Pa) of the four bars; (a) homogeneous; (b) bi-material; (c) tri-layer; (d) smoothly graded.

material interface in the bi-material bar, while a smooth distribution of stress is achieved for the graded bar and tri-layer bar.

With the above observation, we conclude that the material variation has strong influence of the wave pattern. The stress front travels at the speed of the stiffest material, and the stress peak at the stiffer material side can be remarkably higher than the homogeneous case if linear elastic behavior is considered and there is no other source of inelasticity. For example, for the smoothly graded case, the highest stress at the alumina side reaches about 4 times the applied impact traction magnitude.

5. Validation: three-point-bending beams subjected to impact load

This section investigates the influence of material gradation profile on the evolution of stress state, via simulation of a three-point-bending specimen under impact loading, which is based on a *real* material system. The beam is made of glass/epoxy phases. The experiments on material properties and dynamic fracture behavior of this graded specimen have been conducted by Rousseau and Tippur (2000, 2001a,b, 2002a,b). This study offers background knowledge of the dynamic behavior of this material system, as well as a sound understanding of

the stress field in homogeneous and graded materials, which helps to predict the fracture initiation time in specimens of various material gradients.

5.1. Problem description

The three-point-bending specimen under impact loading is illustrated in Fig. 20(a). Due to the symmetry of geometry, material gradation along the y direction and boundary condition, only half of the geometry is modeled for numerical analysis, as shown in Fig. 20(b). The mesh of the uncracked beam problem is plotted in Fig. 21, which is also used for further investigation of fracture behavior using cohesive zone elements (Zhang and Paulino, 2005). The mesh is refined along the center line with uniform element size $h = 92.5$ μm, and the stress variation versus time is retrieved at point P, with coordinates $(x, y) = (0, 0.2W)$, where W is the height of the beam. The point P is of special interest because it corresponds to the crack tip location in other investigations of fracture behavior (Zhang and Paulino, 2005). Hence, the location of interest in this study corresponds to the crack tip location when the crack is present.

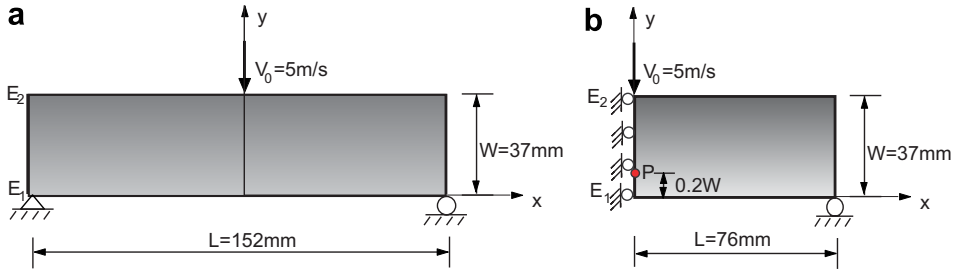

Fig. 20. Epoxy/glass beam subjected to point impact loading; (a) three-point-bending specimen with material gradation along the y-direction; (b) half model with symmetric boundary conditions prescribed. Stress values are retrieved at point P: $(x,y) = (0,0.2W)$.

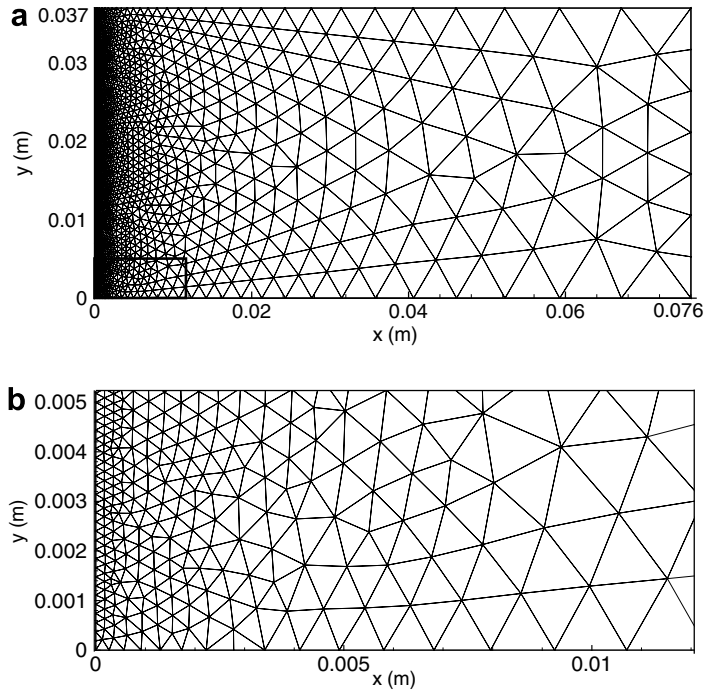

Fig. 21. Discretization of half of the three-point-bending beam model. Mesh contains 7562 nodes and 3647 T6 elements; (a) global mesh; (b) zoom of box region in (a).

5.2. Material gradation

Three simulations are performed considering the following beam configurations under plane stress conditions:

- homogeneous beam ($E_2 = E_1$)
- graded beam stiffer at the impacted surface ($E_2 > E_1$)
- graded beam more compliant at the impacted surface ($E_2 < E_1$)

where subscripts 1 and 2 denote bottom and top surface, respectively. Fig. 22 shows the linear variation of Young's modulus E and mass density ρ for the above three cases. The range of variation is between 4–12 GPa for E, and 1000–2000 kg/m^3 for ρ, which approximates the range of the actual graded specimen material (Rousseau and Tippur, 2002a,b). For the homogeneous beam, the mass density is taken as the mean value of the graded beam counterpart, i.e., 1500 kg/m^3, and the Young's modulus is calculated such that the equivalent E/ρ value equals that of the graded specimen case in an average sense, i.e.,

$$\left(\frac{E}{\rho}\right)_{\text{equiv}} = \frac{1}{W}\int_0^W \frac{E(y)}{\rho(y)}\,\mathrm{d}y, \tag{39}$$

as shown in Fig. 23(a). Thus, the approach from Eq. (39) explains the offset observed in Fig. 22(a) for the homogeneous material modulus ($E_1 = E_2$). Notice that although E and ρ are linear functions of y, the ratio

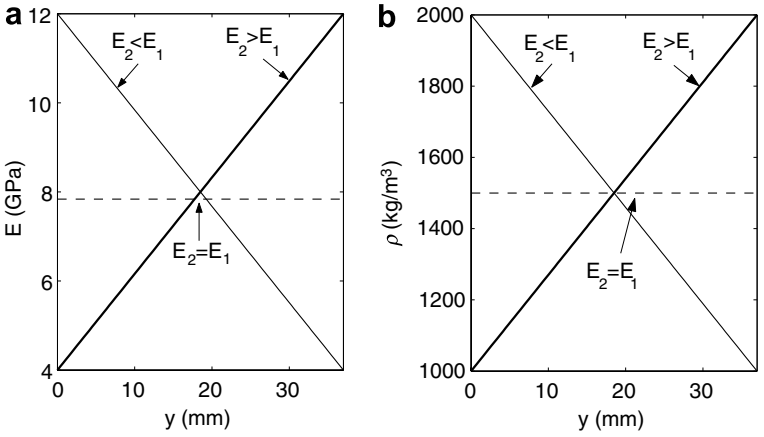

Fig. 22. Variation of (a) Young's modulus E and (b) mass density ρ in homogeneous and graded beams along y direction. The variation of ρ and E are approximated from those provided in Figs. 1 and 2, respectively, of the reference by Rousseau and Tippur (2002b).

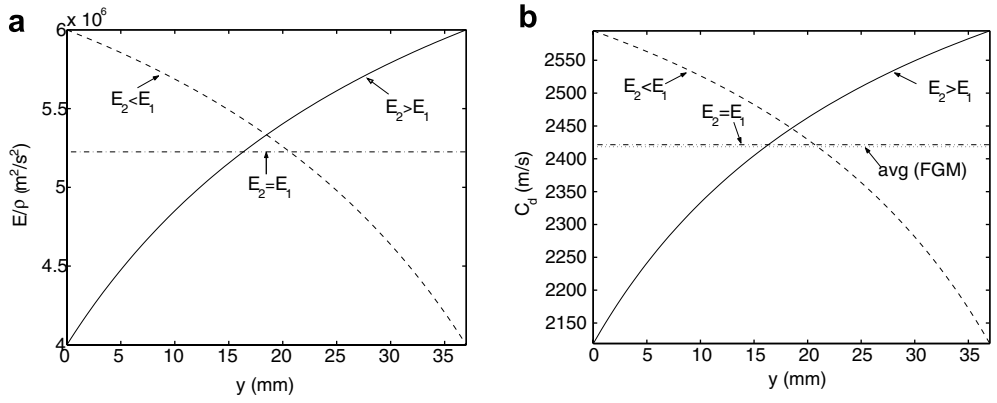

Fig. 23. Variation of (a) E/ρ versus y and (b) dilatational wave speed C_d versus y in homogeneous and graded beams.

E/ρ is not. Poisson's ratio is taken as 0.33 (constant) in all cases. The average dilatational wave speeds (C_d) is defined as

$$(C_d)_{avg} = \frac{1}{W}\int_0^W C_d(y)dy,$$

and the difference for each case is marginal (2421.5 m/s for homogeneous beam, 2418.4 m/s for graded beam, plotted in Fig. 23(b)).

5.3. Results and discussions

When the impact loading is applied at the top surface of the beam, stress waves are generated and propagate towards the lower surface and reflect back at the boundaries. A detailed stress history analysis is helpful to characterize the stress wave behavior accounting for different material gradation profile cases, and also to provide relevant information for predicting beam load bearing capacities. In this section, first the stress results are presented, and then their implication on behavior is discussed, which is facilitated by a statics beam theory analogy. The results for different material profiles are plotted in Figs. 24 and 25 for variation of σ_x and σ_y versus normalized time, respectively.

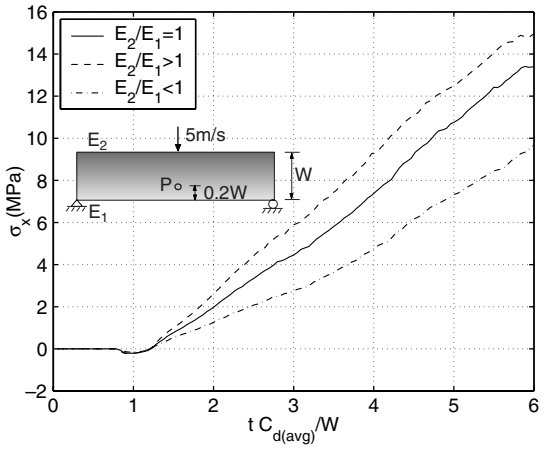

Fig. 24. Stress σ_x at location P: $(x,y) = (0,0.2W)$ in homogeneous and graded beams, with linearly varying elastic moduli, subjected to one point impact by a rigid projectile.

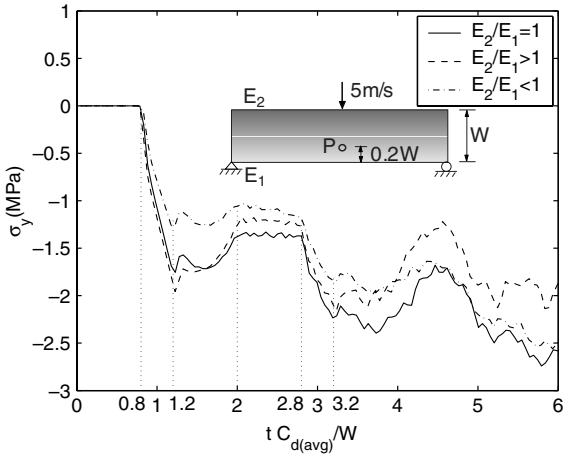

Fig. 25. Stress σ_y at location P: $(x,y) = (0,0.2W)$ in homogeneous and graded beams, with linearly varying elastic moduli, subjected to one point impact by a rigid projectile.

5.3.1. On the stress component σ_x

Fig. 24 indicates that stress component σ_x is primarily dominated by the bending effect. The location of interest (point P in Fig. 20(b)) first experiences stress wave at normalized time 0.8 because the time needed for the first wave front to reach this point is $0.8W/C_d$. This value is exact for homogeneous beam, while for the graded beam, the normalized time is slightly less than 0.8 for the $E_2 > E_1$ case, and slightly larger than 0.8 for the $E_2 < E_1$ case. This is due to the effect of material gradation within the span of the top surface to the location of interest. The difference, though moderate, can be discerned in stress plots of Fig. 24. At this point (normalized time = 0.8), σ_x becomes negative (during normalized time period 0.8–1.3) due to Poission ratio effect, however, this is quickly counterbalanced by the bending effect, and afterwards the stress value increases monotonically with respect to time. Point P in the beam with $E_2/E_1 > 1$ experiences higher tensile stress than in the other two cases.

5.3.2. On the stress component σ_y

The stress component σ_y in Fig. 25 shows strong influence of waves traveling along y direction. The initial stages of this plot can be explained by the dominance of the first batch of propagating waves. At normalized time 0.8, the first tide of compressive wave brings a sharp increase of σ_y in magnitude, as compressive stress. The magnitude of σ_y increases as the subsequent tide of compressive waves pass through point P, till they pass this point again, as tensile wave, after being reflected from the bottom surface at normalized time 1.0. The arrival of the tensile wave at this location, at normalized time 1.2, brings a sharp change of the stress profile towards the opposite direction (magnitude decreases). This trend is sustained for a while till normalized time 2.0, after which the combined effect of subsequent tensile waves that bounced back from the bottom surface, and the compressive waves emanated from the velocity loading, reaches certain balance level at this location, and a "plateau" can be observed from normalized time 2.0–2.8. At normalized time 2.8, the very first tide of stress wave, after being reflected from top surface, again passes through point P, and another cycle of *increase–decrease* in magnitude of σ_y can be observed during normalized time period 2.8–3.2, which is similar to that of time interval 0.8–1.2. Afterwards, the combined effect of the numerous wave tides clouds the influence of any isolated wave, and thus it is difficult to detect the precise time when the σ_y curve changes its trend. Furthermore, waves that traveled to the lateral boundaries also bounce back, adding more complexity to the stress state.

5.3.3. Crack initiation argument

As the load keep increasing, higher stress state in the beam may lead to microcrack and macrocrack formation and finally system failure. Although this study is confined to elastodynamic analysis without considering fracture behaviors, the stress evolution history provides insight on crack initiation characteristics for the three beams described above, through examination of the effect of material gradation on stress levels.

Fig. 26 shows the stress contours for different beams. The region close to the impact loading experiences compressive σ_x, and the central bottom part of the beam experiences tensile σ_x. However, the stress contour patterns are distinctively different for different material gradient cases. First, we notice that close to the top surface, region of compressive σ_x is larger and spans much wider region along x direction for beam with $E_2 > E1$, compared to homogeneous beam (cf. Fig. 26(c) and (b)), and is mostly constricted for beam with $E_2 < E1$ (Fig. 26(a)). This is due to the difference in material stiffness at the loaded region. For beam with $E_2 < E1$, the material is soft under the point load, thus the beam deforms locally and the severe deformation is constricted within a relatively small region. Consequently, the compressive stress region is constricted. For beam with $E_2 > E1$, the material is relatively rigid under the point load, hence the deformation is sustained by nearby region also. Therefore, a larger compressive stress region is developed for beam with $E_2 > E1$ than that for beam with $E_2 < E_1$.

On the other hand, the σ_x value at the central bottom region, being far from the point loading, is dominated by the bending effect. The tensile stress region is larger in the beam with $E_2 > E_1$ than the two other cases, due to different position of neutral axis in each case. To understand the difference in tensile σ_x distribution patterns in the three beams, we resort to first examine a simpler and well-understood problem – a beam subjected to static uniform bending, e.g., the central region of four-point-bending beam.

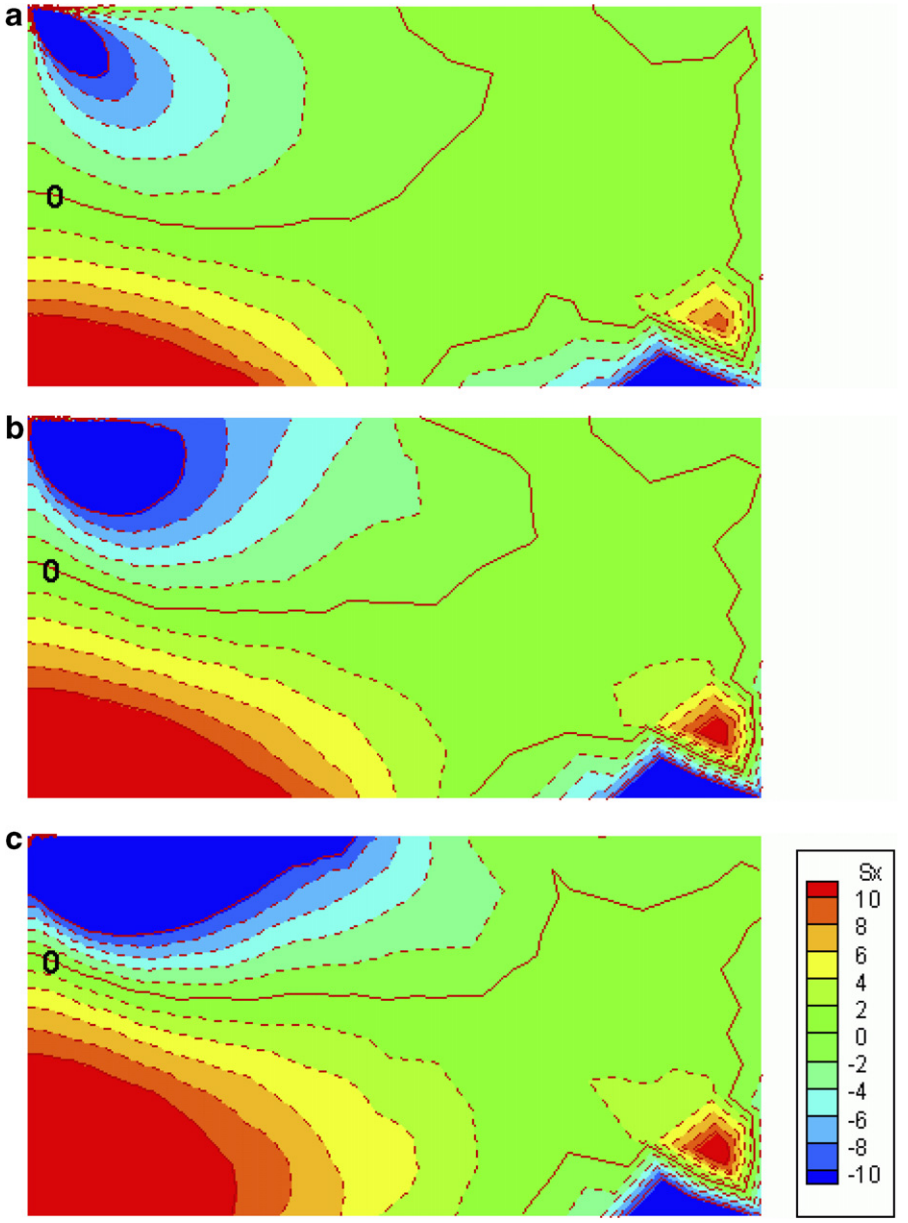

Fig. 26. Effect of material gradient on the contour plot of stress field σ_x for data obtained at time $t = 90$ μs (legend shows σ_x value in MPa). (a) FGM beam with $E_2 < E_1$; (b) homogeneous beam; (c) FGM beam with $E_2 > E_1$.

5.3.4. Statics argument

Consider the stress distribution along y direction in the static case. By enforcing the equilibrium conditions, i.e.,

$$N = \int_0^W \sigma_x(y)\mathrm{d}y = 0, \quad M = \int_0^W \sigma_x(y) y \mathrm{d}y,$$

location of neutral axis can be obtained. In the above expressions, N denotes the summation of normal traction along the beam cross section, and M is the bending moment acting on the cross section of beam. For the homogeneous beam, the neutral axis is located at half height of the beam. For the beam with $E_2 < E_1$, the

material is stiffer at the bottom part, and thus the neutral axis shifts towards the bottom. The opposite situation applies to the beam with $E_2 > E_1$. This speculation can be confirmed by mathematical derivation. A simple calculation reveals that the neutral axis is located at

$$y = 0.415W, \quad \text{for } E_2 < E_1; \qquad y = 0.585W, \quad \text{for } E_2 > E_1$$

for the material gradient considered (Fig. 22). Hence, a larger tensile stress region develops in beam with softer material at bottom ($E_2 > E_1$). At the location of interest, the tensile stress is higher for the beam with $E_2 < E_1$ than that for the beam with $E_2 > E_1$. A simple calculation is carried out here. Assume strain $\epsilon_2 = 0.01$ at top surface. In linear elastic beam with $E_2 > E_1$, the corresponding strain at the bottom surface is $\epsilon_1 = (0.585W/0.415W) \times 0.01 = 0.014097$. At location P: $(x, y = 0, 0.2W)$, σ_x can be obtained as $\sigma_x(P) = E(P)\epsilon(P) = 51.96$ MPa. For the beam with $E_2 < E_1$, with the same assumption of $\epsilon_2 = 0.01$ at top surface, $\epsilon_1 = (0.415W/0.585W) \times 0.01 = 0.007094$ at the bottom surface. At location P: $(x, y = 0, 0.2W)$, σ_x is obtained as $\sigma_x(P) = E(P)\epsilon(P) = 38.22$ MPa.

5.3.5. Statics versus dynamics

The above argument, though made for *static* analysis of linear elastic beam subjected to *uniform bending*, provides an useful analogy for understanding the *dynamic* problem for beam under *point loading*. For a beam subjected to point load, the compressive strain at the top surface is localized under the point load, while the tensile strain develops in a relatively larger region at bottom. The localization of compressive region shifts the neutral axis towards the top surface, as shown in the homogeneous case in Fig. 26(b). Compared to the homogeneous beam, the neutral axis further shifts towards the top surface for FGM beam with $E_2 > E_1$, and shifts towards the bottom surface for FGM beam with $E_2 < E_1$ (cf.Fig. 26(a) and (c) with (b)). This observation is consistent with that made for the static uniform bending beam problem.

5.3.6. Closing remark

The dynamic nature of the problem adds more difficulty to a precise prediction of the stress distribution at certain time, as the neutral axis shifts with respect to time. However, at any specified time, the overall stress distributions in the three beams are similar to those shown in Fig. 26. The above observation implies that the location of interest in the FGM beam with $E_2 > E_1$ is consistently subjected to higher tensile stress than its counterparts. Since the crack initiation is primarily dominated by σ_x, crack initiation would be expected to occur earlier for beam with $E_2 > E_1$. This is confirmed by both the experiment (Rousseau and Tippur, 2002a) and the simulation carried out for fracture analysis (Zhang and Paulino, 2005). It needs to be pointed out, however, that this conclusion assumes identical fracture toughness at the crack tip for the three specimens, which is not true. Fracture toughness depends on local material compositions, which are clearly different for the three cases. This mechanism is considered in the fracture simulation, and the result proves to be consistent with the predictions.

6. Conclusions

This work provides a thorough investigation of wave propagation behavior in smoothly graded heterogeneous material systems considering different material variation profiles. Generalized isoparametric formulation is employed in 2D finite element method to investigate the response of graded material systems under dynamic loading. This formulation adopts the same interpolation methods of the coordinates and displacement to treat material inhomogeneity at the element level. This approach effectively represents the material variation at the element level and results in smooth solution transition across the element boundaries. Explicit updating scheme is adopted to capture the transient response of the material systems under study. With this approach, three classes of problems are examined, including both verification and validation procedures.

Verification procedure is carried out through numerical example of a cantilever beam. Analytical solution for homogeneous problem is employed as reference result to verify the numerical approach. Next, beams with material variation along either x or y directions are investigated. Both Rayleigh–Ritz method and FEM are employed to study the influence of material variation on the fundamental modes and frequencies of the cantilever beam. Results indicate some characteristics particular to the graded material system, including change

of the order of certain modes for different material variation profiles. Moreover, comparison of Rayleigh–Ritz method and FEM results reveals that by simplifying the 2D problem as a 1D model, modes in longitudinal direction is ignored, and may result in a stiffer model.

The second class of problems, which also provides further verification of the computation procedure, consists of investigating wave propagation patterns in fixed-free bars considering homogeneous, bi-material, tri-layered and smoothly graded material profiles, respectively. In bi-material, tri-layered and smoothly graded material beams, wave propagates at the wave speed of the stiffer material, and the stress is much higher at the stiffer side. Moreover, stress history reveals that graded material systems eliminate the stress mismatch present at the sharp bi-material interface. This class of problems also indicate the need for inelastic analysis, which is a topic that deserves further investigation (Zhang and Paulino, 2005).

The validation procedure is performed through simulation of a three-point-bending beam under impact loading, based on real epoxy/glass FGM beam experiment. The numerical results indicate that the tensile stress at location of interest develops at a faster rate for certain material gradation profile ($E_2 > E_1$) than the other cases. This trend is consistent with the experiment observation, and provides important information for predicting structure performance capacity, e.g., crack initiation. The fracture behavior for the polymer-based graded beam has been investigated by the authors (Zhang and Paulino, 2005) using cohesive zone approach, which proves to be consistent with the prediction in the current study.

References

Banks-Sills, L., Eliasi, R., Berlin, Y., 2002. Modeling of functionally graded materials in dynamic analysis. Composites B 33, 7–15.

Bathe, K.-J., 1996. Finite Element Procedures. Prentice-Hall, New Jersey.

Bathe, K.-J., 1999. ADINA-automatic dynamic incremental nonlinear analysis system, Version 7.3, Adina Engineering, Inc. USA.

Chakraborty, A., Gopalakrishnan, J., 2003. A spectrally formulated finite element for wave propagation analysis in functionally graded beams. International Journal of Solids and Structures 40, 2421–2448.

Chin, E.S.C., 1999. Army focused research team on functionally graded armor composites. Materials Science and Engineering A259, 155–161.

Chiu, T.-C., Erdogan, F., 1999. One-dimensional wave propagation in a functionally graded elastic medium. Journal of Sound and Vibration 222, 453–487.

Chopra, A.K., 1995. Dynamics of Structures. Prentice-Hall, New Jersey.

Gazonas, G.A., 2002. Implementation of the Johnson-Holmquist II (JH2) constitutive model into DYNA3D, ARL-TR-2699. Army Research Laboratory, Aberdeen, MD.

Hughes, T.J.R., 1987. The Finite Element Method: Linear Static and Dynamic Finite Element Analysis. Prentice Hall, New Jersey.

Johnson, G.R., Holmquist, T.J., 1994. An improved computational model for brittle materials. In: Schmidt, S.C., Shaner, J.W., Samara, G.A., Ross, M. (Eds.), High Pressure Science and Technology. American Institute of Physics Press, New York, pp. 981–984.

Kim, J.-H., Paulino, G.H., 2002. Isoparametric graded finite elements for nonhomogeneous isotropic and orthotropic materials. ASME Journal of Applied Mechanics 69, 502–514.

Meirovitch, L., 1967. Analytical Methods in Vibrations. The Macmillan Company, New York.

Newmark, N.M., 1959. A method of computation for structural dynamics. ASCE Journal of the Engineering Mechanics Division 85, 67–94.

Parameswaran, V., Shukla, A., 1998. Dynamic fracture of a functionally gradient material having discrete property variations. Journal of Materials Science 33, 3303–3311.

Parameswaran, V., Shukla, A., 2000. Processing and characterization of a model functionally gradient material. Journal of Materials Science 35, 21–29.

Paulino, G.H., Jin, Z.-H., Dodds Jr., R.H., 2003. Failure of Functionally Graded Materials. In: Karihaloo, B. et al. (Eds.), . In: Encyclopedia of Comprehensive Structural Integrity, vol. 2. Elsevier, Amsterdam, pp. 607–644.

Payton, R.G., 1966. Elastic wave propagation in a non-homogeneous rod. The Quarterly Journal of Mechanics and Applied Mathematics 19, 83–91.

Praveen, G.N., Reddy, J.N., 1998. Nonlinear transient thermoelastic analysis of functionally graded ceramic-metal plates. International Journal of Solids and Structures 35, 4457–4476.

Reddy, J.N., 2000. Analysis of functionally graded plates. International Journal for Numerical Methods in Engineering 47, 663–684.

Reddy, J.N., Chin, C.D., 1998. Thermomechanical analysis of functionally graded cylinders and plates. Journal of Thermal Stresses 26, 593–626.

Roache, P.J., 1998. Verification and Validation in Computational Science and Engineering. Hermosa Publishers, Albuquerque, NM.

Rousseau, C.-E., Tippur, H.V., 2000. Compositionally graded materials with cracks normal to the elastic gradient. Acta Materialia 48, 4021–4033.

Rousseau, C.-E., Tippur, H.V., 2001a. Dynamic fracture of compositionally graded materials with cracks along the elastic gradient: experiments and analysis. Mechanics of Materials 33, 403–421.

Rousseau, C.-E., Tippur, H.V., 2001b. Influence of elastic gradient profiles on dynamically loaded functionally graded materials: cracks along the gradient. International Journal of Solids and Structures 38, 7839–7856.

Rousseau, C.-E., Tippur, H.V., 2002a. Evaluation of crack tip fields and stress intensity factors in functionally graded elastic materials: cracks parallel to elastic gradient. International Journal of Fracture 114, 87–111.

Rousseau, C.-E., Tippur, H.V., 2002b. Influence of elastic variations on crack initiation in functionally graded glass-filled epoxy. Engineering Fracture Mechanics 69, 1679–1693.

Santare, M.H., Lambros, J., 2000. Use of a graded finite element to model the behavior of nonhomogeneous materials. Journal of Applied Mechanics 67, 819–822.

Santare, M.H., Thamburaj, P., Gazona, G.A., 2003. The use of graded finite element in the study of elastic wave propagation in continuously nonhomogeneous materials. International Journal of Solids and Structures 40, 5621–5634.

Suresh, S., Mortensen, A., 1998. Functionally Graded Materials. The Institute of Materials, IOM Communications Ltd., London.

Thamburaj, P., Santare, M.H., Gazonas, G.A., 2003. The effect of graded strength on damage propagation in continuously nonhomogeneous materials. Journal of Engineering Materials and Technology 125, 412–417.

Warburton, G.B., 1976. The Dynamical Behaviour of Structures. Pergamon Press, Oxford.

Whittier, L.S., 1965. A note on wave propagation in a nonhomogeneous bar. Journal of Applied Mechanics 32, 947–949.

Zhang, Z., Paulino, G.H., 2005. Cohesive zone modeling of dynamic failure in homogeneous and functionally graded materials. International Journal of Plasticity 21, 1195–1254.